

DOI: 10.1159/000501497

Received: 10/8/2018 2:05:36 AM

Accepted: 6/16/2019

Published(online): 6/17/2019

Added Value of Contrast Medium in Whole-Body Hybrid PET/MRI: Comparison Between Contrast-Enhanced and Non-Contrast-Enhanced Protocols
Celebi F. Cindil E. Sarsenov D. Unalan B. Balci C.

ISSN: 1011-7571 (Print), eISSN: 1423-0151 (Online)

<https://www.karger.com/MPP>

Medical Principles and Practice

Disclaimer:

Accepted, unedited article not yet assigned to an issue. The statements, opinions and data contained in this publication are solely those of the individual authors and contributors and not of the publisher and the editor(s). The publisher and the editor(s) disclaim responsibility for any injury to persons or property resulting from any ideas, methods, instructions or products referred to in the content.

Copyright:

This article is licensed under the Creative Commons Attribution-NonCommercial 4.0 International License (CC BY-NC) (<http://www.karger.com/Services/OpenAccessLicense>). Usage and distribution for commercial purposes requires written permission.

© 2019 The Author(s). Published by S. Karger AG, Basel

Accepted Manuscript

Added Value of Contrast Medium in Whole-Body Hybrid PET/MRI: Comparison Between Contrast-Enhanced and Non-Contrast-Enhanced Protocols

Filiz Celebi^a, Emetullah Cindil^b, Dauren Sarsenov^c, Bulent Unalan^a, Cem Balci^d

Department of ^aRadiology, Gayrettepe Florence Nightingale Hospital, Department of ^bRadiology Gazi University, Departments of ^cGeneral Surgery & ^dNuclear Medicine, Florence Nightingale Hospital, Gayrettepe, Turkey, Department of ^eRadiology, Cleveland Clinic, Lerner School of Medicine, Abu Dhabi, UAE.

Address all correspondence to:

Filiz Çelebi,
Gayrettepe Florence Nightingale Hospital Radiology Department
Cemil Aslan Guder sok. No: 8 Gayrettepe Istanbul
Turkey.

Email: elbuken.filiz@gmail.com

Running Head : Whole Body Hybrid PET/MRI

Key Words: PET/MRI • Malignancy • Fast Protocol • Contrast Medium

Highlights

- A comprehensive oncologic imaging is achieved with PET/MRI when appropriate protocol is used.
- One single examination can cover all organ systems and may detect all types of malignancies.
- A shorter and more accurate Whole Body PET/MRI protocol can be developed for the evaluation of malignancies.

Accepted manuscript

Abstract

Objective: To compare the diagnostic ability and time efficiency of contrast-enhanced (CE) whole body FDG PET/MRI protocol and non-contrast-enhanced (NCE) protocol. **Subjects and Methods:** Ninety-three patients with known primary tumors underwent whole-body hybrid FDG PET/MRI during the follow-up of their malignancies with the use of NCE and CE protocols. The NCE PET/MRI protocol consisted of diffusion-weighted ($b = 0 \text{ s/mm}^2$ and 800 s/mm^2) and T1-weighted Turbo Flash in the axial plane and T2-weighted HASTE sequence in the coronal planes ($\Sigma = 25$ minutes). The CE PET/MRI protocol was performed by acquiring axial serial CE 3D FS VIBE images in the upper abdomen, completing the whole body in late phase in the axial plane ($\Sigma = 30$ minutes). **Results:** There was a statistically significant difference between the total number of lesions detected by the CE protocol (median 2, IQR 0-14) and that detected by the NCE protocol (median 1, IQR 0-5) ($p < 0.001$). More malignancies were detected in the abdomen ($p < 0.001$) and brain ($p < 0.001$) with the CE PET/MRI protocol, whereas no significant difference was present when comparing the two protocols in the detection of malignancies in the head and neck ($p = 0.356$), thorax ($p = 0.09$), lymph nodes ($p = 0.196$) and bone ($p = 0.414$). **Conclusion:** The CE FDG PET/MRI protocol enables fast and accurate detection of malignancies compared to NCE FDG PET/MRI protocol particularly in the upper abdomen and brain. The diagnostic ability and time efficiency can be increased with the proposed short CE protocol in place of the whole body PET/MRI protocol including both NCE and CE imaging sequences.

Introduction

Hybrid positron emission tomography/magnetic resonance imaging (PET/MRI) scanners have the potential to become an effective tool for the evaluation of oncology patients before, during, and after treatment and can influence patient management [1,2]. Hybrid PET/MRI uses PET data to assess the metabolic information of malignant tumors and relies on the uptake of radiotracers. However, certain tumors such as mucinous carcinoma or signet cell-type adenocarcinoma may not reveal the uptake of fluorodeoxyglucose (FDG), which is the most commonly used radiotracer. On the other hand, physiological uptake of FDG in the liver and brain may prevent the depiction of tumors. Therefore, MRI data collected from hybrid PET/MRI systems not only provide superior soft tissue contrast and anatomic detail but may also improve the evaluation of malignant tumors. Therefore, the choice of imaging protocol is crucial for increasing the sensitivity of MRI. The use of intravenous contrast media is essential to oncologic imaging, especially for the detection of malignant tumors in the brain and in the upper abdomen [3-5]. In this study, we investigated whether contrast-enhanced (CE) whole-body PET/MRI protocols increase the sensitivity of detection of malignant tumors compared to non-contrast-enhanced (NCE) protocols.

Subjects and Methods

In our study, 93 consecutive patients with histopathologically proven primary malignant tumors aged between 20-87 were retrospectively evaluated (mean age \pm standard deviation, 55.1 years \pm 14.1) during the period of August 2015 to January 2018. 54 of these patients were men (53.4 \pm 14.7 years), and 39 of them were women (56.4 \pm 13.6 years). The institutional review board approved the study; the requirement of informed consent was waived since the study was a retrospective investigation. The patients referred to PET/MRI from the hematology/oncology and surgery departments as part of the standard oncology imaging were included in the study. Patients

with a history of allergy to gadolinium based contrast agents and end stage renal failure were excluded from the study. All patients had histopathological proof of their primary malignant tumors by surgery (n=56) and/or biopsy (n=37).

Metastatic lesions without histopathologic evidence were identified based on the progression of their size or the appearance of new lesions during follow-up. The malignancy of the lymph nodes was determined based on their size and/or FDG uptake.

Eight patients underwent neoadjuvant therapy, and PET/MRI was performed at follow-up; 45 patients had their primary tumor surgically removed, followed by adjuvant chemotherapy and/or chemoradiotherapy. In 40 patients, the primary tumor was not deemed operable according to the criteria of other imaging modalities, and these patients either underwent chemotherapy and/or chemoradiotherapy.

All patients fasted for at least 6 hours before imaging. The blood glucose level was assessed with a blood glucose meter (OneTouch Vita; LifeScan, Milpitas, California, USA) before imaging to ensure that it was less than 140 mg/dL (7.77 mmol/L).

PET/MRI was performed 45 ± 10 minutes after the injection of FDG (mean dose, 4.54 MBq per kilogram of body weight ± 1 ; range, 370-400 MBq). The images were acquired in supine position on a 3 Tesla Biograph mMR scanner (Siemens Healthcare, Erlangen, Germany) using a 16-channel head and neck surface coil and three 12-channel body coils. These body coils were combined to form a multichannel whole-body coil by using the Total Imaging Matrix technology. The whole-body images were obtained in five to six bed positions according to the size of the patient and each bed time position is kept between 2-2.5 minutes. PET acquisition occurred simultaneously during the whole-body MRI acquisition. In all patients, the whole-body PET/MRI covered the entire body from head to knee. For the attenuation correction, four-point Dixon images were obtained in the coronal plane. The whole-body MRI protocol consisted of both NCE images and CE images and provided the most comprehensive oncologic imaging dataset in the routine in our institution. The imaging stations were arranged consecutively in the caudocranial direction. The comprehensive MRI protocol

that included both CE and NCE studies consisted of T2-weighted single-shot echo train (HASTE) (TR/TE, 1500 msec/87 msec) in the coronal plane, T1-weighted slice-selective Turbo Flash (TR/TE, 1600 msec/2.5 msec) and free breath diffusion-weighted imaging using EPI technique (TR/TE, 12000 msec/78 msec, $b=0$ s/mm² and $b=800$ s/mm²) in the axial planes. After the NCE protocol was performed, a weight-adapted dose of a gadolinium-based contrast agent was administered, and serial CE images were obtained using breath-hold 3D VIBE (TR/TE, 4.56 msec/2.03 msec) in the arterial, portal venous and equilibrium phases covering the upper abdomen in the axial plane. After the serial CE images were acquired, continuous breath-hold 3D VIBE images were obtained from head to knee in the axial plane, and all the sections were combined, resulting in uninterrupted whole-body coverage. Detailed information regarding the whole-body PET/MRI protocol is shown in Table 1. The total scan duration of the PET/MRI examination was 50-60 minutes. The durations of both the NCE and CE protocols were 25-30 minutes.

The images were evaluated by two radiologists; one had 25 years of experience, and the other had 8 years of experience in reading MRI and hybrid imaging. Both readers were blinded to patient data and diagnosis. One research associate separated each study into two parts, and the loaded images had a NCE part and a CE part. The data were analyzed on a dedicated workstation (Syngo Via; Siemens Healthcare, Erlangen, Germany). The NCE and CE protocols were reviewed one month apart to avoid bias. The review of the cases for CE and NCE studies took one hour each. All images with diagnostic quality for PET and MRI were evaluated separately and as fused images, the number of lesions was recorded for both protocols. The radiologists and a nuclear medicine physician evaluated the images in a joint reading session and made consensus. The NCE dataset was evaluated using NCE MR images, PET/MRI fusion images and attenuation-corrected raw data PET images. The CE dataset was evaluated by reviewing CE MR images, fused PET/MRI images and attenuation-corrected raw data PET images.

Statistical analyses were performed using SPSS software version 20. The variables were investigated using visual methods (histograms, probability plots) and analytical methods

(Kolmogorov-Smirnov) to determine whether or not the distribution was normal.

As most of the variables excepting “age” were not represented by real numbers, descriptive analyses for tests were presented using medians and interquartile range (IQR). Friedman’s test was conducted to evaluate whether there is a significant change in the total number of detected lesions among different MRI sequences separately for each anatomic region (due to violations of parametric test assumptions as number of lesions detected can only be integer). Pairwise comparisons were performed using Wilcoxon signed rank test. A p value of less than or equal to 0.05 was accepted as statistically significant.

Results

Of the 93 patients, 17 patients had non FDG-avid malignant tumors. The rest of the patients had FDG avid malignant tumors, 36 patients had distance metastasis (M) and 40 patients had lymph node metastases (N).

Distribution of the primary malignant tumors is shown in Table 2. Gastrointestinal tumors include gastric, pancreatic, colorectal cancers, hepatocellular carcinoma and cholangiocarcinoma.

The number of lesions detected using the CE protocol (median 2, IQR 0 - 14) was significantly higher than that detected using the NCE protocol (median 1, IQR 0 - 5) ($p < 0.001$). The total number of lesions detected using the CE protocol varied between 0 - 120 (minimum-maximum), whereas that detected using the NCE protocol was 0 - 75 (minimum-maximum). The total number of lesions detected with only the PET component (median 1, IQR 0 - 11) was significantly lower than the number of lesions detected with the CE PET/MR protocol (median 2, IQR 0 - 14) ($p < 0.001$).

Regarding the number of region-based lesions, the number of lesions in the brain detected with the CE protocol (median 2, IQR 1 - 2) was significantly higher than that detected with the NCE protocol (median 0, IQR 0-1) ($p = 0.001$, $n = 11$). (Fig. 1)

In the abdomen, the CE PET/MRI protocol (median 2, IQR 1 - 6) was superior to the NCE protocol (median 1, IQR 0-2) ($p < 0.001$, $n = 65$) (Fig. 2).

There was no difference between the number of malignant tumors detected by the two protocols for the head and neck ($p = 0.356$, $n = 13$), bone ($p = 0.414$, $n = 28$), thorax ($p = 0.09$, $n = 31$) (Fig. 3), and lymph nodes ($p = 0.196$, $n = 32$) (Table 3).

Discussion

Our study showed that the CE fast PET/MRI protocol depicted more malignant tumors in the upper abdomen and in the brain compared to the NCE protocol. In addition, our CE fast protocol may increase patient comfort due to its short duration and is an effective tool for the evaluation of oncology patients before, during, and after treatment.

PET/MRI is a new imaging modality that combines the sensitivity of molecular imaging of PET and the superior radiologic diagnostic capabilities of MRI. In addition, PET/MRI provides detailed background anatomical landmarks from MRI images. MRI also bestows superior tissue contrast that helps to localize tumors and assist in the local staging (T staging) of tumors. PET/MR is superior to PET/CT because it resolves soft tissue without the need for radiation exposure. The metabolic information from PET data together with the diagnostic accuracy of CE whole-body MRI may increase the sensitivity of tumor detection.

Several studies have shown that the detection of primary and metastatic liver and brain tumors by MRI is superior to that by PET [3,5]. In liver imaging, serial CE images are essential to depict hypervascular lesions, and only CE images can depict brain metastases [3,4,6-9]. In the pancreas, CE images may depict hypervascular neuroendocrine tumors that are not FDG avid [10-12]. Additionally, renal tumors may be evaluated with CE images to differentiate between benign and malignant lesions [13]. PET images rely on the uptake of FDG, which is taken up physiologically by the tissues of the liver and brain. Primary liver tumors such as HCC can only take up FDG if they are less differentiated [14,15]. In our dataset, CE PET/MRI depicted more HCC with the serial CE images. HCC is a hypervascular tumor with arterial blood supply, and arterial enhancement with venous washout is diagnostic for HCC in serial CE images [8].

In contrast to our results, Lee et al. presented that the effect of gadolinium based contrast agents on PET image can be negligible quantitatively and qualitatively [16]. In imaging renal and bladder tumors, MRI is superior to PET with CE protocols. Renal lesions, including cysts, can only be categorized according to their enhancement pattern [17]. In our dataset, we did not observe any primary renal tumor; however, CE MRI protocols can further help to distinguish between malignant and benign renal lesions. We did not observe any significant difference in bone metastasis and lymph node involvement.

FDG-PET detection of hypometabolic metastasis and increased bone marrow activity after chemotherapy is not sensitive [18-19-20]. Bone marrow-sensitive MRI techniques can provide diagnostic information on FDG-negative cases [21]. Our data showed that the combined evaluation of PET and MRI with either diffusion-weighted imaging (DWI) or post-contrast VIBE equally assessed the bone marrow metastases. Previous studies have shown that CE MRI and DWI have similar sensitivities for the detection of bone metastases [22,23].

Stolzman et al. [24] and Catalano et al. [25] compared lung nodule detection rates using CT, MR and PET either in different combinations or separately. They found similar detection rates for both PET/CT and PET/MRI. Our study revealed similar results for the detection of lung nodules. The duration of the whole-body PET/MRI examination is long, and it is unpleasant for the patient to undergo a one-hour examination in a closed environment. Therefore, shorter protocols have been performed [26,27]. Our CE protocol may be used as standard protocol for shorter examinations, which may increase patient throughput and patient comfort.

The limitation of our study may include the limited number of cases with each malignancies to group and see which particular malignancies may benefit the most for contrast enhanced protocol. Also not all cases were histopathologically proven. Further prospective studies may be needed for tailored PETMRI protocols for specific malignancies especially in terms of local staging. Contrast enhanced studies may be performed with the use of improved temporal resolution to calculate the contrast passage (Ktrans) and monitor the antiangiogenic treatments.

Conclusion

An optimal oncologic imaging was achieved using the appropriate protocol for PET/MRI, and a variety of tumor types and involvement of the organ systems can be reviewed by optimizing the protocol. We investigated the use of the CE whole-body PET/MRI protocol for the assessment of malignant tumors, and our results indicated that MRI with intravenous contrast might increase the sensitivity of PET/MRI. The protocol with the emphasis of CE examination can further shorten the PET/MRI exam with increased detection rate of neoplasms.

Accepted manuscript

References

1. Beomsik K, Jeong ML, Yong SS, Woo S, Hur BY, Jeon JH, et al. Added value of integrated whole body PET/MRI for evaluation of colorectal cancer: Comparison with contrast-enhanced MDCT. *Am J Roentgenol* 2016;206:W10-20.
2. Torigian MD, Zaidi H, Kwee CT, Saboury B, Udupa JK, Cho ZH, et al. PET/MR Imaging: Technical aspects and potential clinical applications. *Radiology* 2013;267:26-44.
3. Kitajima K, Nakamoto Y, Okizuka H, Onishi Y, Senda M, Suganuma N, et al. Accuracy of whole body FDG-PET/CT for detecting brain metastases from non-central nervous system tumors. *Ann Nucl Med* 2008;22:595-602.
4. Lohmann P, Stoffels G, Cecon G, Rapp M, Sabel M, Filss CP, et al. Radiation injury vs. recurrent brain metastasis: combining textural feature radiomics analysis and standard parameters may increase 18F-FET PET accuracy without dynamic scans. *Eur Radiol* 2017;27:2916-2927.
5. Niekel MC, Bipat S, Stoker J. Diagnostic imaging of colorectal liver metastases with CT, MR imaging, FDG PET, and/or FDG PET/CT: a meta analysis of prospective studies including patients who have not previously undergone treatment. *Radiology* 2010;257:674-684.
6. Lee JM, Zech CJ, Bolondi L, Jonas E, Kim MJ, Matsui O, et al. Consensus report of the 4th International forum for Gadolinium-Ethoxybenzyl-Diethylenetriamine Pentaacetic Acid Magnetic Resonance Imaging. *Korean J Radiol* 2011;12:403-415.
7. Lee KH, Lee JM, Park JH, Kim JH, Park JH, Yu MH, et al. MR imaging in patients with suspected liver metastases: value of liver-specific contrast agent gadoxetic acid. *Korean J Radiol* 2013;14:894-904.
8. Di Martino M, Marin D, Guerrisi A, Baski M, Galati F, Rossi M, et al. Intraindividual comparison of gadoxetate disodium-enhanced MR imaging and 64-section multidetector CT in the detection of hepatocellular carcinoma in patients with cirrhosis. *Radiology* 2010;256:806-816.
9. Seo HJ, Kim MJ, Lee JD, Chung WS, Kim YE. Gadoxetate disodium-enhanced magnetic resonance imaging versus contrast-enhanced 18F- Fluorodeoxyglucose positron emission

- tomography/computed tomography for the detection of colorectal liver metastases. *Invest Radiol* 2011;46:548-555.
10. Baumann T, Rottenburger C, Nicolas G, Wild D. Gastroenteropancreatic neuroendocrine tumors (GEP-NET)—imaging and staging. *Best Pract Res Clin Endocrinol Metab* 2016;30:45-57.
 11. Panagiotidis E, Alshammari A, Michopoulou S, Skoura E, Naik K, Maragkoudakis E, et al. Comparison of the impact of 68 Ga-DOTATATE and 18F-FDG PET/CT in clinical management in patients with neuroendocrine tumors. *J Nucl Med* 2017;58:91-96
 12. Dromain C, Deandreis D, Scoazec JY, Goere D, Ducreux M, Baudin E, et al. Imaging of neuroendocrine tumors of the pancreas. *Diagn Interv Imaging*. 2016;97:1241-1257.
 13. Vargas HA, Chaim J, Lefkowitz RA, Lakhman Y, Zheng J, Moskowitz CS, et al. Renal cortical tumors: use of multiphasic contrast-enhanced MR imaging to differentiate benign and malignant histologic subtypes. *Radiology* 2012;264:779-788
 14. Takeuchi S, Rohren EM, Abdel-Wahab R, Xiao L, Morris JS, Macapinlac HA, et al. Refining prognosis in patients with hepatocellular carcinoma through incorporation of metabolic imaging biomarkers. *Eur J Nucl Med Mol Imaging* 2017;44:969-978.
 15. Torizuka T, Tamaki N, Inokuma T, Magata Y, Sasayama S, Yonekura Y, et al. In vivo assessment of glucose metabolism in hepatocellular carcinoma with FDG-PET. *J Nuc Med* 1995;36:1811-1817.
 16. Lee WH, Park JA, Kim KY. Effects of MR contrast agents on PET quantitation in PET-MRI study. *J Nucl Med* May 2011 vol. 52 no. supplement 1 53.
 17. Verma S, Rajesh A, Prasad RS, Gaitonde K, Lall CG, Mouraviev V, et al. Urinary bladder cancer: role of MR imaging. *Radiographics* 2012;32:371-387
 18. Nakai T, Okuyama C, Kubota, Yamada K, Ushijima Y, Taniike K, et al. Pitfalls of FDG-PET for the diagnosis of osteoblastic bone metastases in patients with breast cancer. *Eur J Nucl Med Mol Imaging* 2005;32:1253-1258.

19. Hamaoka T, Madewell JE, Podoloff GN, Hortobagyi GN, Ueno NT. Bone imaging in metastatic breast cancer. *J Clin Oncol* 2004;22:2942-2953.
20. Sugawara Y, Fisher SJ, Zasadny KR, Kison PV, Baker LH, Wahl RL, et al. Preclinical and clinical studies of bone marrow uptake of fluorine-1-fluorodeoxyglucose with or without granulocyte colony-stimulating factor during chemotherapy. *J Clin Oncol* 1998;16:173-180.
21. Schmidt GP, Reiser MF, Baur-Melnyk A. Whole-body imaging of the musculoskeletal system: the value of MR imaging. *Skeletal Radiol* 2007;36:1109-1119
22. Soliman M, Taunk NK, Simons RE, Osborne JR, Kim MM, Szerlip NJ, et al. Anatomic and functional imaging in the diagnosis of spine metastases and response assesment after spine radiosurgery. *Neurosurg Focus* 2017;42:E5.
23. Lecouvet FE, Larbi A, Pasoglou V, Omoumi P, Tombal B, Michoux N, et al. MRI for response assessment in metastatic bone disease. *Eur Radiol* 2013;23:1986-1997.
24. Stolzmann P, Veit-Haibach P, Chuck N, Rossi C, Frauenfelder T, Alkadhi H, et al. Detection rate, location, and size of pulmonary nodules in trimodality PET/CT-MR: comparison of low-dose CT and Dixon-based MR imaging. *Invest Radiol* 2013;48:241-246.
25. Catalano OA, Rosen BR, Sahani DV, Hahn PF, Guimaraes AR, Vangel MG, et al. Clinical impact of PET/MR imaging in patients with cancer undergoing same-day PET/CT: initial experience in 134 patients-a hypothesis-generating exploratory study. *Radiology* 2013;269:857-869.
26. Grueneisen J, Sawichi LM, Schaarschmidt BM, Suntharalingam S, von der Ropp S, Wetter A, et al. Evaluation of a fast protocol for staging lymphoma patients with integrated PET/MRI. *PLoS One* 2016;11:e0157880.
27. Grueneisen J, Schaarschmidt BM, Heubner M, Suntharalingam S, Milk I, Kinner S, et al. Implementation of FAST-PET/MRI for whole –body staging of female patients with recurrent pelvic malignancies: a comparison to PET/CT. *Eur J Radiol* 2015;84:2097-2102.

Table 1: Detailed Whole-Body PET/MRI protocol

NCE protocol	Image plane	Slice thickness (mm)	Gap (%)	Slices (no.)	Acquisition time (min:s)	TR/TE	Matrix	Field of view (mm)	Resolution (mm²)	FA	Breath-hold Method
DWI (b=0 s/mm² and 800 s/mm²)	axial	6	0.6	300	11:25	7200/81	126x128	440	128/100	NA	Breath-free
T1-weighted Turbo flash	axial	5	1	175	6:16	1600/2.46	194x320	450	320/81	20	Resp trigger
T2-weighted HASTE	coronal	5	1	175	5:59	1500/87	320x320	440	320/100	136	Resp trigger
CE protocol	Image plane	Slice thickness (mm)	Gap (%)	Slices (no.)	Acquisition time (min:s)	TR/TE	Matrix	Field of view (mm)	Resolution (mm²)	FA	Breath-Hold Method
3D FS VIBE for upper abdomen	axial	3	0	96	0:23	4.56/2.03	195x320	380	320/75	9	Breath-hold
3D VIBE FS Dixon	coronal	1.90	0	144X5	1:49	4.02/1.23	149x288	460	288/75	9	Breath-hold
3D FS VIBE for the brain	axial	1	0	176	2:30	9.50/3.69	256x320	231	320/80	12	Breath-free

CE: Contrast-enhanced, NCE: Non-contrast-enhanced

Table 2: Distribution of primary malignant tumors

Primary malignant tumors	Number of patients
Hepatobiliary	28
Other Gastrointestinal	16
Genitourinary	10
Breast	18
Immunoproliferative	6
Lung Carcinoma	6
Other	9

Accepted manuscript

Table 3: Distribution of malignant tumors for different body regions

Region	CE protocol		NCE protocol		p
	Median	IQR	Median	IQR	
Brain	2	1-2	0	0-1	p<0.001
Head & Neck	2	1-3.5	2	1-4	p=0.356
LN	1	1-4	1	1-3	p=0.196
Thorax	1	1-4	1	1-3	p=0.09
Abdomen	2	1-6	1	0-2	p< 0.001
Bone	5	1-30	4.5	1-30	p=0.414
Total	2	0-14	1	0-5	p< 0.001

Friedman's test

Figure Legend

Fig. 1. A 56-year-old patient with chronic liver disease. An enhancing nodule is present in segment 6 of the liver in the arterial phase (arrow, a) that reveals contrast washout on the portal venous phase (arrow, b) during the contrast-enhanced PET/MRI protocol. On the diffusion-weighted MRI (c) and PET/MRI fusion images (d), no lesion is visible during the non-contrast-enhanced PETMRI protocol.

Fig. 2. A 67-year-old patient with breast cancer. Non-contrast-enhanced PET/MRI fusion images reveal two FDG-avid lesions in the cerebellum (arrows, a) that are not seen on the diffusion-weighted MRI (b). 3D VIBE postcontrast images acquired using the contrast-enhanced PET/MRI protocol reveal both metastases (white arrows, c) and an additional smaller lesion (black arrow, c).

Fig. 3. A 72-year-old patient with advanced colon cancer. Contrast-enhanced PET/MRI protocol reveals multiple lung metastases and bone involvement in the thoracic vertebra (arrow, a) on the postcontrast 3D VIBE axial image. Non-contrast-enhanced protocol with diffusion-weighted MRI reveals bone involvement (arrow, b) with less apparent lung lesions. Fusion PETMRI images of the non-contrast protocol depicts both lung and bone metastases (arrow, c).

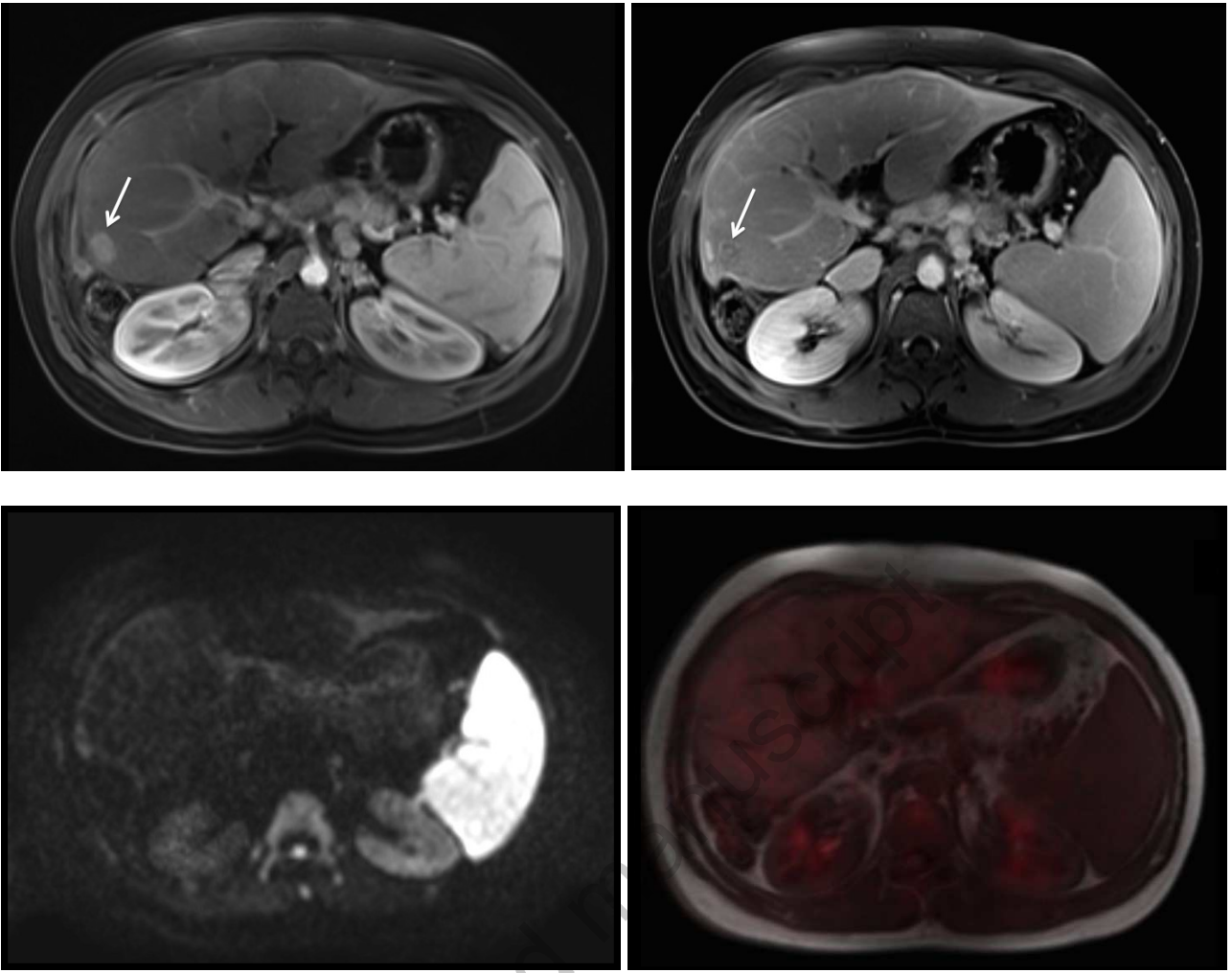


Fig 1 (a-d)

Accepted

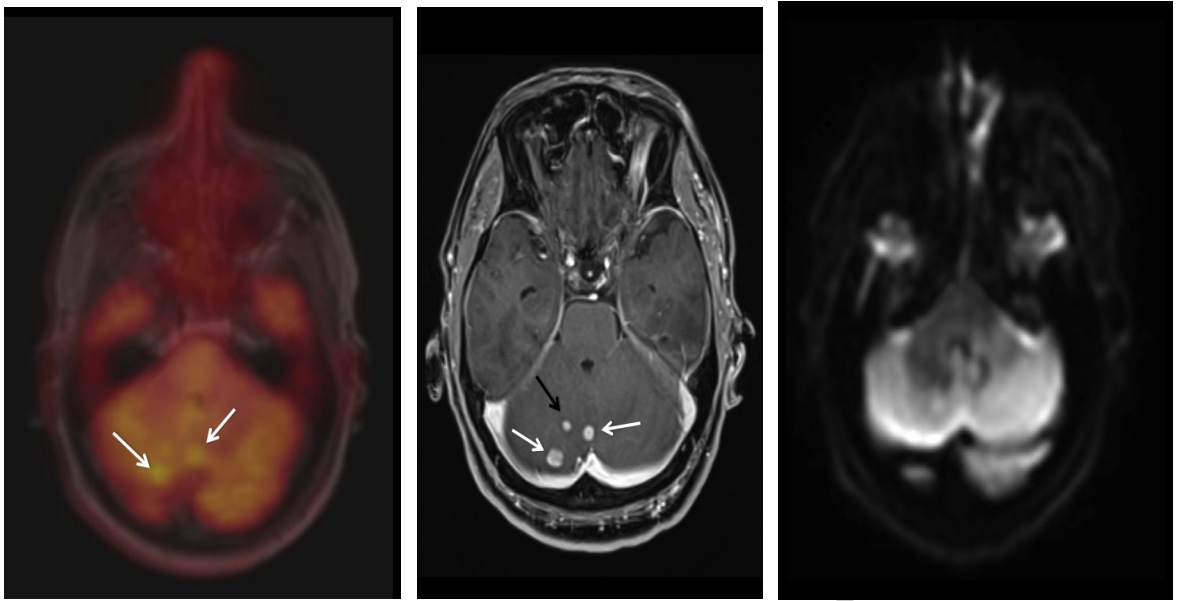


Fig 2 (a –c)

Accepted manuscript

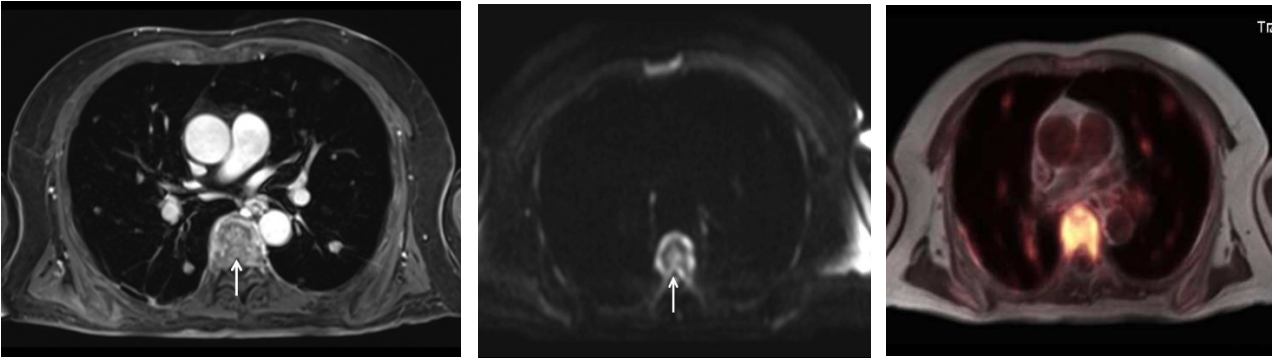


Fig 3 (a – c).

Accepted manuscript